DYNA
http://dyna.medellin.unal.edu.co/

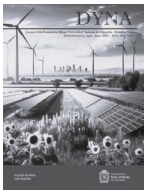

UNIVERSIDAD NACIONAL DE COLOMBIA

A new thin-film solar cell prototype based on Na-doped $BiFeO_3$

Adán de Jesús Bautista-Morantes, Carlos Ordulio Calderón-Carvajal, Jairo Alberto Gómez-Cuaspud & Enrique Vera-López

Universidad Pedagógica y Tecnológica de Colombia, Instituto para la Investigación e Innovación en Ciencia y Tecnología de Materiales – INCITEMA, Tunja, Colombia. adan.bautista@uptc.edu.co, carlos.calderon02@uptc.edu.co, jairo.gomez01@uptc.edu.co, enrique.vera@uptc.edu.co

Received: January 24th, 2025. Received in revised form: March 14th, 2025. Accepted: March 31st, 2025

Abstract
The development of thin film photovoltaic devices based on third and fourth generation materials has attracted the attention of the scientific community worldwide, finding the need to experiment among different assemblies and structurally modified materials to find the best efficiency of converting solar energy into electrical energy. Therefore, in this work, the efficiency of three prototypes of thin-film photovoltaic perovskite solar cells (PSCs) constructed using three sodium-doped samples of $BiFeO_3$ as absorber layers has been evaluated. The assembly was carried out based on an *n-i-p* architecture obtaining thin-films with glass/ITO/CdS/perovskite/Au/Mo/glass general configuration. The study has led to the conclusion that the efficiency of the assembled photovoltaic devices increases with the insertion of sodium and that the proposed configuration is functional for the construction of thin-film perovskite solar cells (PSCs).

Keywords: Perovskite; ferroelectricity; voltage-current; *p*-type doping; efficiency.

Un nuevo prototipo de célula solar de capa fina basada en $BiFeO_3$ dopado con Na

Resumen
El desarrollo de dispositivos fotovoltaicos de película delgada basados en materiales de tercera y cuarta generación ha atraído la atención de la comunidad científica mundial, encontrando la necesidad de experimentar entre diferentes ensamblajes y materiales estructuralmente modificados para encontrar la mejor eficiencia de conversión de energía solar en energía eléctrica. Por ello, en este trabajo se ha evaluado la eficiencia de tres prototipos de células solares fotovoltaicas de capa delgada de perovskita (PSCs) construidas utilizando tres muestras dopadas con sodio de $BiFeO_3$ como capa absorbente. Los ensamblajes se realizaron en base a una arquitectura *n-i-p* obteniéndose películas delgadas con configuración general vidrio/ITO/CdS/perovskita/Au/Mo/vidrio. El estudio ha permitido concluir que la eficiencia de los dispositivos fotovoltaicos ensamblados aumenta con la inserción de sodio y que la configuración propuesta es funcional para la construcción de células solares de capa delgada de perovskita (PSCs).

Palabras clave: Perovskita; ferroelectricidad; tensión-corriente; dopaje tipo *p*; eficiencia.

1 Introduction

In recent decades, the design of photovoltaic devices has attracted the attention of many researchers around the world, as the development of new configurations and cell types has grown exponentially, with promising results for better utilization of solar energy sources and their conversion into electrical energy [1]. In order to find a more efficient device, numerous studies have been developed exploring different prototypes, such as the thin-film solar cell, which is still being experimented with [2]. The most developed thin-film solar cells have used three main materials as the absorber layer: amorphous silicon (α-Si), cadmium telluride (CdTe), and copper indium gallium selenide (CIGS) [3]. However, some limitations have been found for each of these systems, such as photon scattering and its rapid degradation when interacting with light (Staebler-Wronski effect) in α-Si based cells [4,5], the high cost of manufacturing CdTe devices given that tellurium (Te) is a scarce element in nature and that Cd is a primary element of high toxicity [3,6]. On the other hand, indium (In) used in CIGS thin-films, is also a scarce element in nature,

How to cite: Bautista-Morantes, A.deJ., Calderón-Carvajal, C.O., Gómez-Cuaspud, J.A., and Vera-López, E., A new thin-film solar cell prototype based on Na-doped BiFeO3. DYNA, 92(237), pp. 30-37, April - June, 2025.

and compounds such as H_2Se, are a source of highly toxic selenium (Se), so its use should be limited [3,7].

To overcome the limitations of traditional cells, recent work has investigated a variety of materials for use in third- and fourth-generation devices [8,9]. Among these are perovskites of ABX_3 structure, which readily absorb light and carry charge when illuminated by a light source. Due to their high dielectric constants, high absorption coefficient [10], low bond excitation energy [11], ferroelectric properties [12,13] and other chemical and physical properties, perovskites are promising materials for the design of photovoltaic and optoelectronic devices [9].

The conventional architecture of a perovskite solar cell (PSC) is either planar *n-i-p* (FTO/ETL/perovskite/HTL/metal) or planar *p-i-n* (FTO/HTL/perovskite/ETL/metal). In both cases, particles from the HTL or ETL layers can be added to the active layer (mesoporous structures): FTO is the photoanode layer (glass or ITO, a transparent conductive composite), HTL corresponds to the hole carrier layer (p-type layer usually based on NiO, Cu_xO, MoO_X, etc.). The *i*-layer is a perovskite or absorber material with ABX_3 structure, ETL is the electron transport layer (n-type layer usually based on TiO_2, ZnO, SnO_2, CdS, etc.) and the last layer is a conductive metal or back electrode such as Au, Ag or Al [8,9,14–19]. This type of cell works when the photons irradiated by a source interact with the perovskite layer, which absorbs the energy, allowing the generation of excitons that separate into electrons and holes, creating a potential difference that moves towards the electrodes of the diode-type system, thus converting solar energy into electrical energy [8,9,12,14].

The efficiency of PSCs depends on several variables related to the architecture and the physical, chemical and electrical properties of the materials in the different layers. Their electrical, optical and magnetic properties such as bandgap, conductivity and resistance phenomena are determined by the structure, composition and morphology of the material. $BiFeO_3$ (BFO) is one of the perovskites whose structure can be modified by p-type and *n*-type cation doping in order to improve its electrical and optoelectronic behavior for use as an absorber layer. Some doping includes the insertion of alkaline earth, transition and rare earth cations at the A and B positions [20–34]. The *p*-type doping of BFO with Na atoms has been explored and found to decrease the optical bandgap values and increase the electrical conductivity, making this type of material promising for the design of PSCs [27,35].

In the present study, three photovoltaic devices with glass/ITO/CdS/perovskite/Au/Mo/glass architecture (*n-i-p* configuration; where *i* and *p* are only from perovskite) were assembled, alternating three BFO samples doped with 0 %, 8 % and 10 % sodium in the A position. To evaluate the efficiency of the new solar cells constructed by modifying the conventional PSC architecture, they were designed using undoped BFO or BFO samples doped with different sodium ratios (abbreviated NaBFO) as the absorber layer. The cells were electrically characterized to determine the influence of the structural and morphological properties of each perovskite sample on the conversion efficiency of the devices.

This study presents a novel approach by introducing Na doping, which has not been systematically investigated in BiFeO-based solar cells. The research shows that Na incorporation significantly enhances carrier mobility and reduces recombination losses, resulting in improved photovoltaic performance. This work fills a critical gap in the field of photovoltaics by establishing a direct correlation between Na doping concentration and efficiency improvements, providing a new way to optimize $BiFeO_3$ based materials in development of PSCs.

1.1 Key Contributions

The key contributions of this study are as follows:

i. First systematic study of Na doping in $BiFeO_3$ thin-film solar cells with this general configuration, demonstrating its impact on efficiency enhancement.
ii. Improved photovoltaic performance, showing a significant increase in open-circuit voltage (Voc) and short-circuit current (Jsc) compared to undoped $BiFeO_3$.
iii. Fabrication of a prototype solar cell, to demonstrate the feasibility of Na-doped $BiFeO_3$ for practical applications.

2 Materials and Methods

The cells assembled in this work were fabricated based on the architecture described in Fig. 1; (glass/ITO/CdS/perovskite/Au/Mo/glass) with an interlayer contact area of 80 mm^2 (10 mm x 8 mm). A photovoltaic flat glass plate manufactured by Yilin Glass Manufacturing Co., Ltd. with a thickness of 2 mm, visible light reflectance of 7.30 %, visible light transmittance of 91.60 % without anti-reflective (AR) coating, ultraviolet (UV) transmittance of 86.80 % and total solar heat gain coefficient of 93.20 % was used as the top substrate. The deposition of the ITO (top contact), Au (back contact) and Mo layers were performed by sputtering technique in a Three-head DC/RF sputtering magnetron, model CY-MSP300S-RFDC, CYKY brand, assisted by argon plasma. Each layer was deposited at a power of 70 W, with a pressure of $1.3x10^{-3}$ Pa for 20 min at room temperature, obtaining 270 nm thick layers from sputtering targets with 99.99 % purity purchased from Plasmaterials.

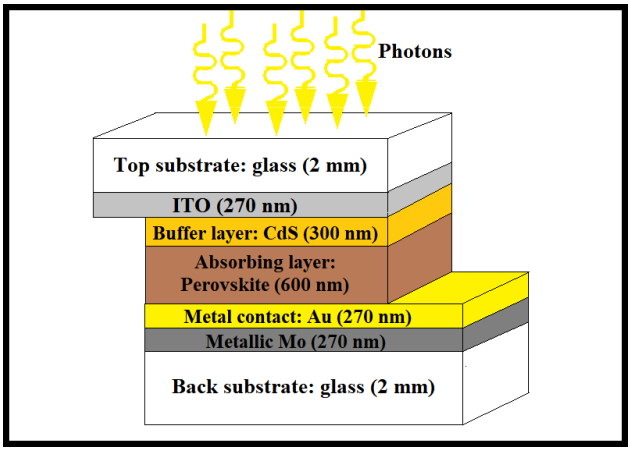

Figure 1. Architecture of the solar cells assembled in this work.
Source: the authors

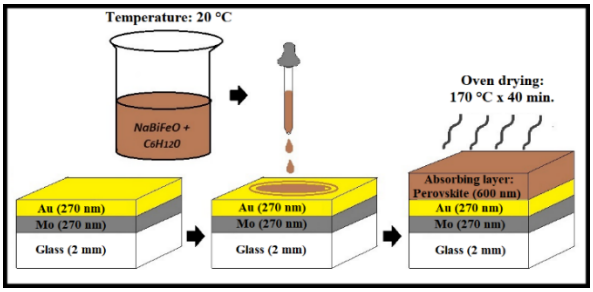

Figure 2. Deposition by drop casting technique for the buffer layer and the selected NaBFO adsorbent layer.
Source: the authors

The buffer and adsorbent layers were deposited using the drop-casting technique of A. Kumar *et al.* [36], as shown in Fig. 2. The buffer layer was deposited suspending CdS powders (98 % pure, Thermo Scientific Chemicals) in cyclohexanol (99 % pure, Thermo Scientific Chemicals), the heterogeneous mixture was drop-cast onto the ITO layer at room temperature and the liquid was evaporated at 170 °C for 40 minutes to control the coffee ring effect (CRE) [37]. Three layers were deposited by the same method until a homogeneous deposit of 300 nm thickness was obtained.

In this study, the drop-casting technique was selected for the deposition of the buffer layer on the Na-doped $BiFeO_3$ thin films due to specific material considerations. Since the Na-doped $BiFeO_3$ was synthesized in bulk form, alternative deposition methods such as thermal evaporation were not suitable, as they could induce structural changes, leading to secondary phase formation and potential loss of Na doping. In addition, spin coating was considered inappropriate due to the large grain size of the synthesized material, which would result in uneven film distribution. Furthermore, both undoped and Na-doped $BiFeO_3$ exhibit intrinsic magnetic properties that could interact with the electromagnetic fields present in certain deposition systems, potentially affecting film uniformity and composition. Therefore, drop-casting was chosen as the most suitable method to ensure homogeneous film formation while maintaining the integrity of the doped $BiFeO_3$ structure.

Thus, a 600 nm absorber layer was deposited using one of the three previously synthesized doped BFO samples with different concentrations of sodium, allowing three different cells to be assembled. Each sample used and its structural, morphological and electrical properties are detailed in Table 1 and are the result of previous characterizations performed by the authors of this work [35]. Finally, a lower substrate of glass was placed as a back support of the cell with the same characteristics as the upper substrate and the low resistance contacts were soldered.

The electrical characterization of the deposited cells was performed using a Thorlabs MCWHL5 photodiode of 470 nm at 6500 K and 840 mW, coupled to a GAMRY 1010 potentiostat-galvanostat interface. The electrical response was measured with Keithley 2450 SourceMeter® equipment by the voltage-current method (I vs. V) generating the electrical signals from the incidence of the 470 nm light beam with a maximum irradiance of 24.8 μW/mm^2 at a distance of 30 mm over the cross-sectional area of the cell of 80 mm^2 area, which produced an effective irradiance of 24.6 μW/mm^2 calculated by Lambert's law [38].

Table 1.
Summary of all variables and measurements of the NaBFO samples package deposited as active layer in this work (ʊ = S).

Sample	Na doped (%)	Purity (%)
NaBFO-00	0	100
NaBFO-08	8	69.34
NaBFO-10	10	63.95
Sample	**Main phase**	**Impurity phase**
NaBFO-00	$BiFeO_3$	-----
NaBFO-08	$Na_{0.08}Bi_{0.92}FeO_{3-\delta}$	$Bi_2Fe_4O_9$
NaBFO-10	$Na_{0.10}Bi_{0.90}FeO_{3-\delta}$	$Bi_2Fe_4O_9$
Sample	**Microdeformations main phase**	**Oxygen Vacancies main phase = δ**
NaBFO-00	2.10 x 10^{-4}	----
NaBFO-08	5.17 x 10^{-4}	8.40 x 10^{-2}
NaBFO-10	9.54 x 10^{-4}	10.50 x 10^{-2}
Sample	**Mean particle diameter (μm)**	**Indirect optical bandgap (eV)**
NaBFO-00	11.26	2.77
NaBFO-08	13.57	2.15
NaBFO-10	9.72	2.12
Sample	**Conductivity (S m^{-1})**	**Warburg diffusion element (ʊ s$^{1/2}$)**
NaBFO-00	1.15 x 10^{-5}	2.28 x 10^{-8}
NaBFO-08	4.75 x 10^{-5}	8.38 x 10^{-7}
NaBFO-10	1.36 x 10^{-4}	8.01 x 10^{-6}

Source: the authors

The GAMRY 1010 potentiostat-galvanostat interface has a reported accuracy of ±1.0 mV (2 %) for voltage measurements and ±3 pA (3 %) for current readings, while the Keithley 2450 SourceMeter® instrument has percent basic accuracy at 6½-digit resolution for voltage and current. Both instruments were calibrated to the manufacturer's specifications using certified reference cells and standard resistance benchmarks to ensure data reliability.

To ensure reliability, all electrical measurements were performed in triplicate for each sample. The reported voltage and current values represent the average of the three independent measurements. Since no significant oscillations or variations were observed in the data, error measures were not included in the graphical presentation. The consistency of the measurements indicates the reproducibility of the results and confirms the stability of the Na-doped $BiFeO_3$ thin films under tested conditions.

The I-V measurements reported by the instruments allowed the determination of the listed parameters and the calculating of the cell efficiency (η_{eff}) using eq. (1) [14]:

- ✓ Maximum current (I_{MAX}) and voltage (V_{MAX}).
- ✓ Maximum power (P_{MAX}).
- ✓ Open circuit voltage (V_{OC}).
- ✓ Short circuit current (I_{SC}).

$$\eta_{eff} = \frac{V_{OC} * I_{SC} * FF}{I_{sun} * A_L} \quad (1)$$

Where FF is the fill factor – eq. (2), I_{sun} indicates the luminous intensity applied on the cell and A_L is the area of the cell radiated [39].

$$FF = \frac{V_{MAX} * I_{MAX}}{V_{OC} * I_{SC}} \quad (2)$$

3 Results and Discussion

Fig. 3 shows the I-V curve obtained for the thin-film cell with NaBFO-00 absorber layer without Na doping. The electrical parameters obtained from the curve and the instrument are given in Table 2. The behavior of the diode-type system is typical of a semiconductor, whose behavior is attributed to the absorber layer (synthesized BFO) and the cell configuration (glass/ITO/CdS/NaBFO-00/Au/Mo/glass).

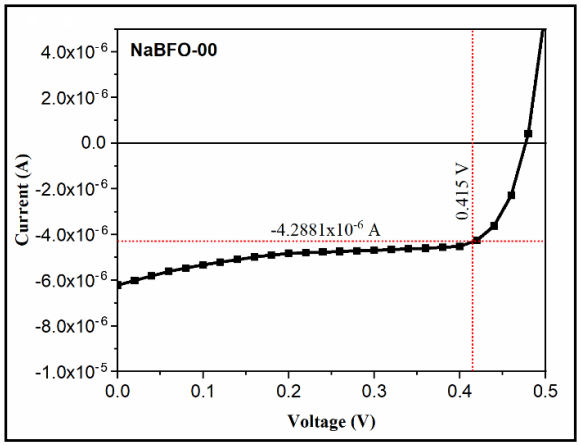

Figure 3. I-V curve for the cell with NaBFO-00 absorber layer.
Source: the authors

Table 2.
Electrical parameters of the cell with NaBFO-00 absorber layer.

Parameter		Magnitude	Units
Open circuit voltage	V_{oc}	476.10	mV
Short circuit current	I_{sc}	6.17 x 10^{-3}	mA
Maximum power	P_{max}	1.78	µW
Voltage at maximum power point	V_m	415.00	mV
Current at maximum power point	I_m	4.29 x 10^{-3}	mA

Source: the authors

Fig. 4 shows the I-V curve obtained for the thin-film cell with NaBFO-08 absorber layer, 8 % sodium doped material (configuration: glass/ITO/CdS/NaBFO-08/Au/Mo/glass). The electrical parameters resulting from the curve and also provided by the equipment are shown in Table 3.

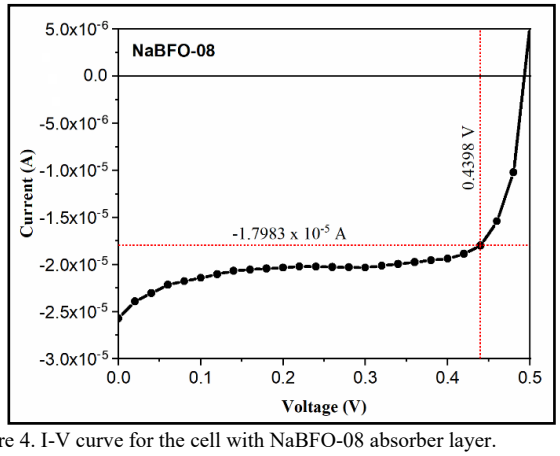

Figure 4. I-V curve for the cell with NaBFO-08 absorber layer.
Source: the authors

Table 3.
Electrical parameters of the cell with NaBFO-08 absorber layer.

Parameter		Magnitude	Units
Open circuit voltage	V_{oc}	492.80	mV
Short circuit current	I_{sc}	2.57 x 10^{-2}	mA
Maximum power	P_{max}	7.91	µW
Voltage at maximum power point	V_m	439.80	mV
Current at maximum power point	I_m	1.80 x 10^{-2}	mA

Source: the authors

Fig. 5 shows the I-V curve obtained for the thin-film cell with NaBFO-10 absorber layer, 10 % sodium doped material (configuration: glass/ITO/CdS/NaBFO-10/Au/Mo/glass). The electrical parameters resulting from the curve and also provided by the instrument are shown in Table 4.

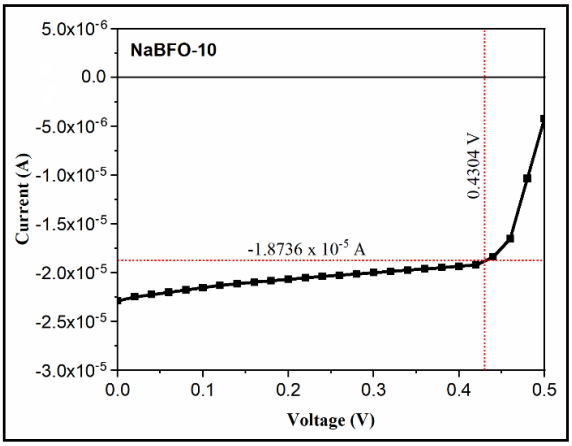

Figure 5. I-V curve for the cell with NaBFO-10 absorber layer.
Source: the authors

Table 4.
Electrical parameters of the cell with NaBFO-10 absorber layer.

Parameter		Magnitude	Units
Open circuit voltage	V_{oc}	510.50	mV
Short circuit current	I_{sc}	2.28 x 10^{-2}	mA
Maximum power	P_{max}	8.06	µW
Voltage at maximum power point	V_m	430.40	mV
Current at maximum power point	I_m	1.87 x 10^{-2}	mA

Source: the authors

The measured parameters recorded in Table 2 to Table 4 were mathematically conducted by means of eq. (1) and eq. (2), and the efficiency value for each assembled cell was obtained (Table 5).

Table 5.
Electrical measurements of irradiated cells.

Absorbent layer material	V_{oc} (mV)	I_{sc} (mA)	P_{max} (µW)	FF (%)
NaBFO-00	476.10	6.17 x 10^{-3}	1.78	0.61
NaBFO-08	492.80	2.57 x 10^{-2}	7.91	0.62
NaBFO-10	510.50	2.28 x 10^{-2}	8.06	0.69

Absorbent layer material	I_{sun} (µW/mm²)	A_L (mm²)	η (%)
NaBFO-00	24.60	80	9.04 x 10^{-2}
NaBFO-08	24.60	80	0.40
NaBFO-10	24.60	80	0.41

Source: the authors

Table 6.
Efficiency of undoped BFO solar cells reported in the literature.

Author	Cell structure	I_{sun} (mW/cm^2)	η (%)	Ref.
O. Ceballos-Sánchez et al.	glass/ITO/CdS/ BFO-Thin/PbS/Ag	100	7.65 x 10^{-3}	[40]
Z. Xie et al.	flexible-mica/$SrRuO_3$/BFO/Au	455	3.1 x 10^{-2}	[41]
Z. Fan, K. Yao, and J. Wang	Si/SiO_2/Ti/Pt/BFO/ZnO/FTO	22.3	0.33	[42]
S. Chatterjee, A. Bera, and A. J. Pal	glass/ITO/NiO/ BFO/ZnO/Al	100	9.8 x 10^{-2}	[32]
H. Sattarian, T. Tohidi, and Sh. Rahmatallahpur	glass/ITO/CdS/ PbS/Al	90	1.31	[43]

Source: the authors

According to the values obtained for the efficiency of each cell and recorded in Table 5, an increase in the solar conversion efficiency is observed with the doping of the doped BFOs used as absorber layer; therefore, the stoichiometric increase of Na^+ ions, caused the decrease of the electrochemical resistance of the material and improved the electrical conductivity in proportion to the increase of oxygen vacancies and the structural defects generated in the main phase by the presence of the larger host cation as recorded in Table 1. On the other hand, the resistive effect of the material associated with the purity, size and boundary of the sintered grains increased, resulting in a lower electron flow reflected in an increase of only 0.01 % in efficiency between the cell with 8 % and 10 % Na doping.

The efficiency values obtained for the cell (glass/ITO/CdS/NaBFO-00/Au/Mo/glass) with a NaBFO-00 or BFO absorber layer without Na doping are within the average range of the values obtained by other authors as shown in Table 6.

The difference between the reported values and those obtained for the undoped BFO cell assembled in this work are attributed to the structural defects together with the morphological properties of the synthesized BFO, the measurement conditions and the constructive form of the cell, finding an efficiency very similar to that obtained by S. Chatterjee, A. Bera, and A. J. Pal, with values of 9.8 x 10^{-2} % for the glass/ITO/NiO/BFO/ZnO/Al assembly [32]. The glass/ITO/CdS/NaBFO-00/Au/Mo/glass thin-film structure favored the efficiency with respect to other designs reported in the literature, since the molybdenum and gold layers received the unabsorbed photons and refracted them to the absorber layer, favoring a higher interaction between the *p*-type material and the photons per unit area irradiated [44,45]. On the other hand, the transparent conductive oxide (ITO) and the gold metal contact favored the flow of electrons in the circuit since its function as electrodes induced low electrical resistance. In addition, the contact area between the electrodes and the *p-n* junction was established as the same size, improving the conduction of the cell. Likewise, the thickness ratio of the *p-n* layers had an impact on the final efficiency of the cell, since the potential difference in the diode depends on this parameter, similarly the thickness had a 2:1 ratio of BFO:CdS, which guaranteed the best efficiency in the measurement conditions [46].

Given the same design conditions between the cells with Na-doped BFO absorber layer and the cell with undoped BFO, the differences in efficiency are attributed to the structural and morphological variables compared in Table 1 for the synthesized materials, finding a direct relationship between the increase in efficiency and the sodium ratio. The increase of sodium induced a lack of charges in the system and the formation of a doped stable phase, in which oxygen vacancies were formed and its equilibrium is described by the Kröger-Vink notation recorded in eq. (3) and eq. (4), showing repercussions in the vacancies concentration in the synthesized systems. Despite this, the measurements in the cell show a better behavior in the more doped material, which means that a higher density of vacancies prevailed in this system, producing an increase in the conductivity that generates efficient potential differences, favoring the recombination processes; reason why an efficiency of 0.40 was obtained for the cell with the BFO doped with 8 % Na and 0.41 for the cell doped with 10 % Na [47].

$$Na_2O \rightarrow 2(Na_{Bi})^{"} + O_O^X + 4h^{\cdot} \quad (3)$$

$$Fe^{2+} + \frac{1}{3}V_{O}^{\cdot\cdot} + \frac{1}{3}h^{\cdot} \rightarrow Fe^{3+} + V_{O}^{\cdot\cdot} \quad (4)$$

Where *NaBi* corresponds to the substitution of a sodium atom (Na) by a bismuth atom (Bi), O_O^X is the released oxygen that could enter the structure or be released to the environment as $O_{2(g)}$, h refers to the hole-type charge carriers, V_O are the oxygen vacancies [35].

On the other hand, the reduction of the optical bandgap of the Na-doped BFO was the variable that most determined the efficiency, since the energy required to move electrons from the valence band to the conduction band was significantly lower. Aspects such as particle size and reduced purity induced resistive phenomena in the cells, so that the difference in the efficiency measure between the systems constructed with sodium-doped absorber layers is minimal, since the presence of a secondary phase with higher bandgap values limited the number of electrons available in the conduction layer, as well as the resistance generated by the grain boundary associated to materials, limiting the recombination processes.

The efficiencies measured for NaBFO-08 and NaBFO-10 respectively, are consistent with the increase in efficiency reported by other authors when $BiFeO_3$ is doped with cations such as Al, Cr, Cu, Ti, La, Pr, Nd, and Gd [21,22,31,48]. Thus, it is concluded that, given the conditions under which the cells were synthesized and manufactured; doping the BFO with 10% sodium increases its efficiency by approximately 0.32%, which corresponds to 3.53 times the efficiency of the undoped BFO cell.

Under the measurement conditions, there is a dispersion between the light waves reflected by the molybdenum, gold and perovskite layers, and the same waves emitted by the light source, but despite these light interaction phenomena, the measurement was standardized at a distance of 30 mm,

since at this distance no dispersive variations were observed in the trends shown in Fig. 5. In addition, the indirect bandgap values of the perovskite samples used as the absorber layer in this study ranged from 2.12 to 2.77 eV, so that according to the empirical relationship proposed by J. K. Singh, S. K. Mandal and G. Banerjee [49], an increase in refractive index (*n*) values between 2 and 3 units can be estimated, which contributed to the reflection losses and led to a decrease in light absorption by the Na-doped BFO samples [50]. Likewise, it is possible to improve the fabrication process by depositing all the layers preferably by the sputtering method, which, will allow a precise control of the morphological homogeneity in each layer of the cell.

The observed increase in efficiency due to Na doping can also be attributed to changes in the electronic bands structure of the $BiFeO_3$. While no previous theoretical studies have explicitly reported the band structure, defect density, or carrier concentration for Na-doped $BiFeO_3$, the experimental results provide indirect evidence for these effects. The reduction in the optical bandgap observed in Table 1 suggests a narrowing of the energy difference between the valence and conduction bands, which facilitates carrier excitation and improves photovoltaic performance. In addition, the improvement in device efficiency implies an increase in defect density, which in turn could contribute to a higher carrier concentration by introducing shallow donor cations. These effects are consistent with previous reports on aliovalent doping in perovskite oxides, where the introduction of cations leads to electronic structure modifications and defect engineering. Future theoretical studies, such as density functional theory (DFT) calculations, may provide further insight into the precise role of Na in tuning the electronic properties of $BiFeO_3$. However, extended stability assessments, such as prolonged exposure to humidity, temperature fluctuations, and continuous light illumination, are required to fully evaluate a complete behavior mechanism of these materials. Possible challenges include Na diffusion, phase segregation, or interfacial degradation that could affect long-term performance, as well as the study of accelerated aging tests in-situ with spectroscopic techniques would provide deeper insights into the stability of Na-doped $BiFeO_3$ solar cells.

Finally, this work allowed for the calculation of the efficiency of light conversion into electrical energy of three perovskite cells, in which samples doped with 0 %, 8 % and 10 % sodium were used as the active layer. It was observed that the efficiency increases with the insertion of the host cation and that the differences are a consequence of the purity, morphology and structures of the phases present in the material, so that perovskites of the $Na_{(x)}Bi_{(1-x)}.FeO_{3-\delta}$ type are an alternative to consider for the study of second and third generation photovoltaic devices. In addition, it was possible to verify that the cell architecture is functional and has efficiencies similar to those found by other researchers for $BiFeO_3$-based cells.

4 Conclusions

The efficiency of thin-film cells assembled with Na-doped BFO samples as the absorber layer, allowed for the conclusion that the insertion of the host cation improves the electrical and optoelectronic properties of the BFO for its use in design of solar cells. An increase of 0.32 % in efficiency was found when the BFO was doped with 10 % sodium which allowed obtaining a cell with an approximate efficiency of 0.41 % for the glass/ITO/CdS/NaBFO-10/Au/Mo/glass assembly, so that the sample with 63.95 % of the $Na_{0.10}Bi_{0.90}FeO_{2.895}$ phase is the sample used in this work with better structural properties for the construction of PSCs. Therefore, the hypothesis formulated in this work is accepted and it is confirmed that the structural modification of BFO with Na atoms improves the efficiency of perovskite-based thin-film absorber layer photovoltaic devices.

The *n-i-p* configuration (where *i* and *p* are formed only by perovskite) proposed in this work was functional, comparing the measured values with those reported by other authors using similar architectures *p-i-n* and *n-i-p* type along different layers. For future work, it is recommended to explore alternative thin-film solar cell structures, where the *p-i-n* junction is standardized to favor the recombination processes and to control the interaction between the irradiated light and the reflected light due to reflective phenomena in the cell.

References

[1] Lee, T.D., and Ebong, A.U., A review of thin film solar cell technologies and challenges. Renewable and Sustainable Energy Reviews, 70, pp. 1286–1297, 2017. DOI: https://doi.org/10.1016/j.rser.2016.12.028.

[2] Zeman, M., and Schropp, R.E.I., 1.17 - Thin-Film Silicon PV Technology. Comprehensive Renewable Energy, A. Sayigh, Ed., Oxford: Elsevier, 2012, pp. 389–398. DOI: https://doi.org/10.1016/B978-0-08-087872-0.00119-0.

[3] Efaz, E.T. et al., A review of primary technologies of thin-film solar cells. Engineering Research Express, 3(3), art. 032001, 2021. DOI: https://doi.org/10.1088/2631-8695/ac2353.

[4] Tanimoto, H., Arai, H., Mizubayashi, H., Yamanaka, M. and Sakata, I., Light-induced hydrogen evolution from hydrogenated amorphous silicon: Hydrogen diffusion by formation of bond centered hydrogen. J Appl Phys, 115(7), art. 073503, 2014. DOI: https://doi.org/10.1063/1.4865166.

[5] Schüttauf, J.W. et al., Amorphous silicon–germanium for triple and quadruple junction thin-film silicon based solar cells. Solar Energy Materials and Solar Cells, 133, pp. 163–169, 2015. DOI: https://doi.org/10.1016/j.solmat.2014.11.006.

[6] Candelise, C., Winskel, M. and Gross, R., Implications for CdTe and CIGS technologies production costs of indium and tellurium scarcity. Progress in Photovoltaics: Research and Applications, 20(6, pp. 816–831, 2012. DOI: https://doi.org/10.1002/pip.2216.

[7] Fthenakis, V.M. and Moskowitz, P.D., Thin-film Photovoltaic Cells: Health and Environmental Issues in their Manufacture Use and Disposal. Progress in Photovoltaics: Research and Applications, 3(5, pp. 295–306, 1995. DOI: https://doi.org/10.1002/pip.4670030504.

[8] Khalid, S., Sultan, M., Ahmed, E. and Ahmed, W., Chapter 1 - Third-generation solar cells. Emerging Nanotechnologies for Renewable Energy, Elsevier, 2021, pp. 3–35. DOI: https://doi.org/10.1016/B978-0-12-821346-9.00019-5.

[9] Rehman, F. et al., Fourth-generation solar cells: a review. Energy Advances, 2(9), pp. 1239–1262, 2023. DOI: https://doi.org/10.1039/D3YA00179B.

[10] Faridi, A.W. et al., Synthesis and Characterization of High-Efficiency Halide Perovskite Nanomaterials for Light-Absorbing Applications. Ind Eng Chem Res, 62(11, pp. 4494–4502, 2023, DOI: https://doi.org/10.1021/acs.iecr.2c00416.

[11] Bello, S., Urwick, A., Bastianini, F., Nedoma, A.J. and Dunbar, A., An introduction to perovskites for solar cells and their characterisation. Energy Reports, 8, pp. 89–106, 2022. DOI: https://doi.org/10.1016/j.egyr.2022.08.205.

[12] Li, H. et al., Photoferroelectric perovskite solar cells: Principles, advances and insights. Nano Today, 37, p. 101062, 2021. DOI: https://doi.org/10.1016/j.nantod.2020.101062.

[13] Röhm, H., Leonhard, T., Schulz, A.D., Wagner, S., Hoffmann, M.J. and Colsmann, A., Ferroelectric Properties of Perovskite Thin Films and Their Implications for Solar Energy Conversion. Advanced Materials, 31(26), art. 1806661, 2019. DOI: https://doi.org/10.1002/adma.201806661.

[14] Luo, Q., 8 - Applications in photovoltaics. Solution Processed Metal Oxide Thin Films for Electronic Applications, Z. Cui and G. Korotcenkov, Eds., Elsevier, pp. 109–140, 2020. DOI: https://doi.org/10.1016/B978-0-12-814930-0.00008-6.

[15] Zhao, Q., Zhou, B., Luo, L., Duan, Z., Xie, Z. and Hu, Y., A literature overview of cell layer materials for perovskite solar cells. MRS Commun, 2023. DOI: https://doi.org/10.1557/s43579-023-00467-7.

[16] Hossain, M.K. et al., An extensive study on multiple ETL and HTL layers to design and simulation of high-performance lead-free $CsSnCl_3$-based perovskite solar cells. Sci Rep, 13(1), art. 2521, 2023. DOI: https://doi.org/10.1038/s41598-023-28506-2.

[17] Shpatz, A., and Etgar, L., Study of electron transport layer-free and hole transport layer-free inverted perovskite solar cells. Solar RRL, 6(1), art. 2100578, 2022. DOI: https://doi.org/10.1002/solr.202100578.

[18] Dong, J. et al., Efficient perovskite solar cells employing a simply-processed CdS electron transport layer. J Mater Chem C Mater, 5(38), pp. 10023–10028, 2017. DOI: https://doi.org/10.1039/C7TC03343E.

[19] Luo, C. et al., Constructing CdS-based electron transporting layers with efficient electron extraction for perovskite solar cells. IEEE J Photovolt, 11(4), pp. 1014–1021, 2021. DOI: https://doi.org/10.1109/JPHOTOV.2021.3077445.

[20] Shetty, C., Veena Devi Shastrimath, V. and Bairy, R., Tuning the structural, morphological and optical properties of Sr-doped BFO thin films. Phase Transitions, 95(3), pp. 202–211, 2022. DOI: https://doi.org/10.1080/01411594.2022.2032056.

[21] Renuka, H. et al., Enhanced photovoltaic response in ferroelectric Ti-doped BFO heterojunction through interface engineering for building integrated applications. Solar Energy, 225, pp. 863–874, 2021. DOI: https://doi.org/10.1016/j.solener.2021.08.002.

[22] Raj, A. et al., Comparative analysis of 'La' modified BiFeO3-based perovskite solar cell devices for high conversion efficiency. Ceram Int, 49(1), pp. 1317–1327, 2023. DOI: https://doi.org/10.1016/j.ceramint.2022.09.112.

[23] Gebhardt, J. and Rappe, A.M., Doping of $BiFeO_3$: a comprehensive study on substitutional doping. Phys Rev B, 98(12), art. 125202, 2018. DOI: https://doi.org/10.1103/PhysRevB.98.125202.

[24] Chang, S., Chen, C., Jiang, X., Zhao, C. and Chen, J., Improved chemical defects, domain structure and electrical properties of $BiFeO_3$–$BaTiO_3$ lead-free ceramics by simultaneous Na/Bi codoping and quenching process. Ceram Int, 49(10), pp. 16191–16198, 2023. DOI: https://doi.org/10.1016/j.ceramint.2023.01.217.

[25] Mao, W. et al., Effect of Ca doping on photovoltaic effect of $BiFeO_3$. Applied Physics A, 127(7), art. 508, 2021. DOI: https://doi.org/10.1007/s00339-021-04651-1.

[26] Wang, X. et al., Novel electrical conductivity properties in Ca-doped $BiFeO_3$ nanoparticles. Journal of Nanoparticle Research, 17(5), art. 209, 2015. DOI: https://doi.org/10.1007/s11051-015-3018-1.

[27] Zhang, H. et al., Novel behaviors of multiferroic properties in Na-Doped $BiFeO_3$ nanoparticles. Nanoscale, 6(18), pp. 10831–10838, 2014. DOI: https://doi.org/10.1039/C4NR02557A.

[28] Li, J. and Guan, X.Y., Structural and optical properties of Ce doped $BiFeO_3$ nanoparticles via sol–gel method. Micro Nano Lett, 14(13), pp. 1307–1311, 2019. DOI: https://doi.org/10.1049/mnl.2019.0236.

[29] Tang, P., Cao, M., Yu, J., Wang, L. and Zhang, D., Influence of Ba–Cr substitution on structural, optical and magnetic properties of nanocrystalline $BiFeO_3$. Journal of Materials Science: Materials in Electronics, 32(8), pp. 11028–11042, 2021. DOI: https://doi.org/10.1007/s10854-021-05762-4.

[30] Ameer, S., Jindal, K., Tomar, M., Jha, P.K. and Gupta, V., Effect of Li doping on the electronic and magnetic properties of $BiFeO_3$ by first principles. Integrated Ferroelectrics, 193(1), pp. 123–128, 2018. DOI: https://doi.org/10.1080/10584587.2018.1514875.

[31] Kumar, A.M., Peter, I.J., Ramachandran, K., Mayandi, J. and Jayakumar, K., Influence of Al-Cu doping on the efficiency of $BiFeO_3$ based perovskite solar cell (PSC). Mater Today Proc, 35, pp. 62–65, 2021. DOI: https://doi.org/10.1016/j.matpr.2019.05.454.

[32] Chatterjee, S., Bera, A. and Pal, A.J., p–i–n Heterojunctions with $BiFeO_3$ Perovskite Nanoparticles and p- and n-Type Oxides: Photovoltaic Properties. ACS Appl Mater Interfaces, 6(22), pp. 20479–20486, 2014. DOI: https://doi.org/10.1021/am506066m.

[33] Sharma, S., Reshi, H.A., Siqueiros, J.M. and Raymond Herrera, O., Stability of rhombohedral structure and improved dielectric and ferroelectric properties of Ba, Na, Ti doped $BiFeO_3$ solid solutions. Ceram Int, 48(2), pp. 1805–1813, 2022. DOI: https://doi.org/10.1016/j.ceramint.2021.09.261.

[34] Si, S., Deng, H., Wang, T., Yang, P. and Chu, J., Structural phase transition, optical bandgap, interband electronic transition, and improved magnetism in bivalent Ca-, Sr-, Pb-, and Ba-doped $BiFeO_3$ ceramics. Journal of Materials Science: Materials in Electronics, 31(11), pp. 8464–8471, 2020. DOI: https://doi.org/10.1007/s10854-020-03381-z.

[35] Bautista-Morantes, A.B., Calderón-Carvajal, C.O., Gómez-Cuaspud, J.A. and Vera-López, E., Synthesis of $Na_{0.02}Bi_{0.98}FeO_{3-\delta}$ through the standardized preparation of $BiFeO_3$. Mater Sci Energy Technol, 2023. DOI: https://doi.org/10.1016/j.mset.2023.10.003.

[36] Kumar, A., Shkir, M., Somaily, H.H., Singh, K.L., Choudhary, B.C. and Tripathi, S.K., A simple, low-cost modified drop-casting method to develop high-quality $CH_3NH_3PbI_3$ perovskite thin films. Physica B Condens Matter, 630, art. 413678, 2022. DOI: https://doi.org/10.1016/j.physb.2022.413678.

[37] Kumar, A., Zhang, Y., Li, D. and Compton, R.G., A mini-review: How reliable is the drop casting technique? Electrochem commun, 121, art. 106867, 2020. DOI: https://doi.org/10.1016/j.elecom.2020.106867.

[38] Kambezidis, H.D., 3.02 - The Solar Resource. Comprehensive Renewable Energy (Second Edition), T. M. Letcher, Ed., Oxford: Elsevier, pp. 26–117, 2022. DOI: https://doi.org/10.1016/B978-0-12-819727-1.00002-9.

[39] Markvart, T. and Castañer, L., Chapter I-1-A - Principles of solar cell operation. McEvoy's Handbook of Photovoltaics (3rd Ed.). Academic Press, 2018, pp. 3–28. DOI: https://doi.org/10.1016/B978-0-12-809921-6.00001-X.

[40] Ceballos-Sanchez, O. et al., Study of $BiFeO_3$ thin film obtained by a simple chemical method for the heterojunction-type solar cell design. J Alloys Compd, 832, art. 154923, 2020. DOI: https://doi.org/10.1016/j.jallcom.2020.154923.

[41] Xie, Z. et al., Photovoltaic, photo-impedance, and photo-capacitance effects of the flexible (111) $BiFeO_3$ film. Appl Phys Lett, 115(11), art. 112902, 2019. DOI: https://doi.org/10.1063/1.5120484.

[42] Fan, Z., Yao, K. and Wang, J., Photovoltaic effect in an indium-tin-oxide/ZnO/$BiFeO_3$/Pt heterostructure. Appl Phys Lett, 105(16), art. 162903, 2014. DOI: https://doi.org/10.1063/1.4899146.

[43] Sattarian, H., Tohidi, T. and Rahmatallahpur, Sh., Effect of TEA on characteristics of CdS/PbS thin film solar cells prepared by CBD, [Online]. Materials Science-Poland, 34, pp. 540–547, 2016. [visit: January 25, 2025], Available at: https://api.semanticscholar.org/CorpusID:100354693.

[44] Rashid, H. et al., Physical and electrical properties of molybdenum thin films grown by DC magnetron sputtering for photovoltaic application. Results Phys, 14, art. 102515, 2019. DOI: https://doi.org/10.1016/j.rinp.2019.102515.

[45] Hajjiah, A., Badran, H., Kandas, I. and Shehata, N., Perovskite solar cell with added Gold/Silver Nanoparticles: enhanced optical and electrical characteristics. Energies (Basel), 13(15), art. 153854, 2020. DOI: https://doi.org/10.3390/en13153854.

[46] Lakmal, A.A.I., Kumarasinghe, R., Seneviratne, V.A., Thanihaichelvan, M. and Dassanayake, B.S., Effect of CdS layer thickness on thermally evaporated-CdS/CdTe solar cell efficiency. Journal of Materials Science: Materials in Electronics, 33(19), pp. 15627–15637, 2022. DOI: https://doi.org/10.1007/s10854-022-08467-4.

[47] Hubbard, S., Recombination. Photovoltaic Solar Energy, 2016, pp. 39–46. DOI: https://doi.org/10.1002/9781118927496.ch5.

[48] Khan, M. et al., Improving the efficiency of dye-sensitized solar cells based on rare-earth metal modified bismuth ferrites. Sci Rep, 13(1), art. 3123, 2023. DOI: https://doi.org/10.1038/s41598-023-30000-8.

[49] Singh, J.K., Mandal, S.K., and Banerjee, G., Refractive index of different perovskite materials. J Mater Res, 36(9), pp. 1773–1793, 2021. DOI: https://doi.org/10.1557/s43578-021-00257-8.

[50] Kim, M.S., Lee, J.H. and Kwak, M.K., Review: surface texturing methods for solar cell efficiency enhancement. International Journal of Precision Engineering and Manufacturing, 21(7), pp. 1389–1398, 2020. DOI: https://doi.org/10.1007/s12541-020-00337-5.

A. de J. Bautista-Morantes, holds a BSc. Eng. in Electrical Engineering from the Universidad Nacional de Colombia. He holds a PhD. in Engineering and Materials Science from the Universidad Pedagógica y Tecnológica de Colombia, a MSc. in Engineering with an emphasis in Electrical Engineering from the Universidad Industrial de Santander, and a Sp. in Industrial Automation from the Universidad Pedagógica y Tecnológica de Colombia. He is currently an Associate Professor in the Faculty of Engineering at the Universidad Pedagógica y Tecnológica de Colombia and is an active researcher at the Instituto para la Investigación e Innovación en Ciencia y Tecnología de Materiales (INCITEMA). His research focuses on the influence of structural and morphological variables on the optical and electrical response of Na-doped BFOs. He is also interested in industrial process automation and the analysis of complex electrical systems.
ORCID: 0009-0008-1025-8554

C.O. Calderón-Carvajal, holds a BSc. in Chemistry from the Universidad Pedagógica y Tecnológica de Colombia, where he completed his thesis entitled "Theoretical and Experimental Study of the Structural Properties of $Ce_xPr_{(1-x)}O_{2-\delta}$ Materials (x = 0.0; 0.2; 0.4; 0.6; 0.8; 1.0, δ = 0.0)". He is currently pursuing a PhD. in Engineering and Materials Science at the same institution. Additionally, he also holds a specialization in Big Data from the Universitat de Barcelona, which he completed through Coursera. He works as an adjunct Professor at the Universidad Pedagógica y Tecnológica de Colombia and is an active researcher at the Instituto para la Investigación e Innovación en Ciencia y Tecnología de Materiales (INCITEMA). His research focuses on simulation, theoretical development, and experimental testing for the design and characterization of new materials with potential applications in various scientific and industrial fields.
ORCID: 0000-0003-3978-7691

J.A. Gómez-Cuaspud, received a BSc. in Chemistry from the Universidad de Nariño, Pasto, in 2003 and a PhD. in Chemical Sciences from the Universidad Nacional de Colombia, Bogotá, in 2010. From 2010 to 2012, he conducted postdoctoral research at the Universidade Federal do Rio de Janeiro (UFRJ), Brazil, focusing on the development of novel materials for energy storage applications and advanced characterization techniques for solid-state photovoltaic devices. Since 2013, he has been affiliated with the Instituto para la Investigación e Innovación en Ciencia y Tecnología de Materiales (INCITEMA), where he continues his work in materials chemistry. In 2023, he received a B.Sc. in Mathematics from the Universidad Pedagógica y Tecnológica de Colombia, Tunja. His research interests include condensed matter chemistry, materials chemistry, and spectroscopic analysis, especially in the elucidation of structural, morphological, and optoelectronic properties of photovoltaic materials for electrochemical applications. In addition, his interests in mathematics include mathematical modeling and complex data analysis.
ORCID: 0000-0002-9645-516X

E. Vera-López, received a BSc. in Physics in 1990 and a MSc. in Physics in 1994, both from the Universidad Industrial de Santander, Bucaramanga. He received his PhD. in Physics in 1998 from the Ruprecht-Karls-Universität Heidelberg, Germany. Since 2001, he has been as a full-time professor at the Instituto para la Investigación e Innovación en Ciencia y Tecnología de Materiales (INCITEMA), at the Universidad Pedagógica y Tecnológica de Colombia. His research interests include electrochemistry, materials engineering, and the development of coatings and thin films. He currently holds the position of Rector of the Universidad Pedagógica y Tecnológica de Colombia.
ORCID: 0000-0003-4150-9308